Acta Crystallographica Section A
Foundations of Crystallography
ISSN 0108-7673

Received 26 July 2011
Accepted 13 September 2011

Computer-simulated X-ray three-beam pinhole topographs for spherical silicon crystals

Kouhei Okitsu

Nano-Engineering Research Center, Institute of Engineering Innovation, Graduate School of Engineering, The University of Tokyo, 2-11-16 Yayoi, Bunkyo-ku, Tokyo 113-8656, Japan. Correspondence e-mail: okitsu@soyak.t.u-tokyo.ac.jp

X-ray three-beam pinhole topograph images for spherical silicon crystals were computer-simulated based on the *n*-beam Takagi–Taupin (T–T) equation. They were compared with those for parallel-plate crystals. The procedure to integrate the *n*-beam T–T equation for a crystal with an arbitrary shape has been validated in a separate paper [Okitsu *et al.* (2011), *Acta Cryst.* A**67**, 550–556] from comparison between experimentally obtained and computer-simulated six-beam pinhole topographs for a channel-cut silicon crystal.

1. Introduction

One of the difficulties when solving the X-ray dynamical diffraction theory is how to deal with the complex shape of the crystal. The most widely known Ewald–Laue dynamical diffraction theory can be solved only for crystals whose surfaces are planar. In a separate paper (Okitsu *et al.*, 2011), the present author and his coauthors have presented qualitative and quantitative agreements between experimentally obtained and computer-simulated pinhole topographs for a channel-cut silicon crystal. This result shows the efficiency of the method in solving the *n*-beam Takagi–Taupin equation (Okitsu, 2003; Okitsu *et al.*, 2003, 2006) using incident spherical-wave X-rays for a crystal with a complex shape.

Incidentally, it has been recognized for many years that *n*-beam diffraction is one of the candidates to physically phase the structure factors of crystals, which were reviewed by several authors (Colella, 1995*a*,*b*; Chang, 1998, 2004; Weckert & Hümmer, 1997, 1998; Shen, 2005). For applying this *n*-beam method to solving the phase problem, the most proper and convenient shape to be approximated for a crystal whose structure is to be solved is probably a sphere. In the following section, computer-simulated pinhole topographs for spherical silicon crystals are shown together with those for parallel-plate crystals.

2. Computer-simulated pinhole topographs

The procedure for obtaining computer-simulated pinhole topograph images shown in the present paper is fundamentally the same as that described in §3 of Okitsu (2003) and §3 of Okitsu *et al.* (2006).

Figs. 1(*a*) and 1(*b*) show three-beam pinhole topographs computer-simulated with a photon energy of 12.0 keV for parallel-plate silicon crystals whose thicknesses are 75 µm and 7.5 µm, respectively. The computing time for obtaining (*a*), (*b*), (*c*) and (*d*) of Fig. 1 was about 80 min each using four CPUs (16 cores) of the SGI Altix ICE 8400EX supercomputer system. Reflection vectors **h** (0 4 4) and **g** (4 4 0) were assumed to be parallel to the surfaces of the crystals. The assumed polarization state was σ for the **h** reflection. The amplitude profiles of the **h**-reflected X-rays whose intensities are shown in Figs. 1(*a*) and 1(*b*) were Fourier-transformed to obtain the rocking curves shown in Figs. 1 [*S*(*b*)] and 2 [*S*(*b*)] of Ishiwata *et al.* (2010; hereafter denoted IOI 2010). Reflection parameters used for the simulations were the same as those summarized in Table 1 of IOI 2010. Whereas Pendellösung fringes or oscillations can be observed in Fig. 1 [*S*(*b*)] of IOI 2010 and Fig. 1(*a*), such oscillatory profiles were not found in Fig. 2 [*S*(*b*)] of IOI 2010 and Fig. 1(*b*). While the former case does not satisfy the condition mentioned by Weckert & Hümmer (1998) that the thickness of the crystal should be sufficiently small compared with the Pendellösung distance if the phase information were to be extracted (see Table 1 of IOI 2010), the latter case does.

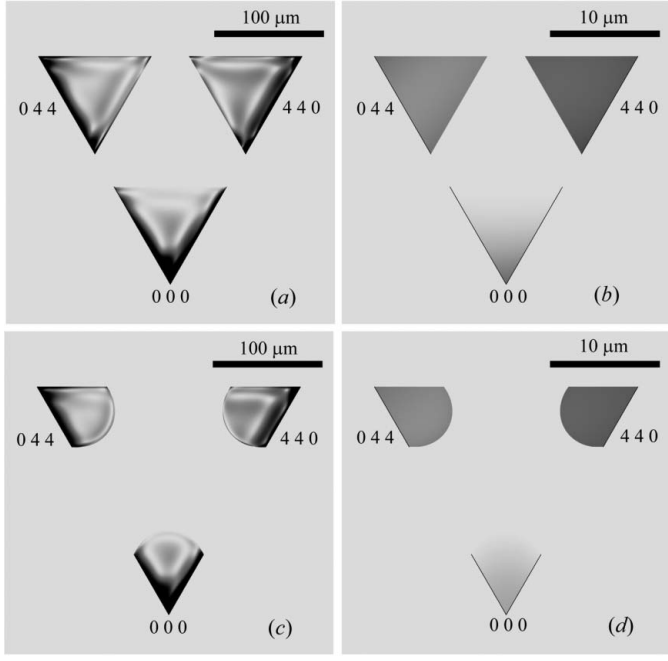

Figure 1
Computer-simulated pinhole topographs for parallel-plate silicon crystals with thicknesses of 75 µm (*a*) and 7.5 µm (*b*), and those for spherical crystals whose diameters are 75 µm (*c*) and 7.5 µm (*d*). **h** (0 4 4) and **g** (4 4 0) reflection vectors were assumed to be parallel to the entrance surface of the crystal. Incident X-rays with a photon energy of 12.0 keV and a polarization state of σ for the **h** reflection were assumed. Imaging plates were assumed to be placed 100 µm [for (*a*) and (*c*)] and 10 µm [for (*b*) and (*d*)] behind the crystals such that **h** and **g** were parallel to the imaging plates.

On the other hand, Figs. 1(*c*) and 1(*d*) were obtained for spherical silicon crystals whose diameters are 75 μm and 7.5 μm, respectively. The center of the sphere S_c was placed such that the direction r_e–S_c was parallel to $-\mathbf{h} \times \mathbf{g}$, where r_e is the incidence point of the X-rays. Surprisingly, it can be found that the patterns observed in topograph images simulated for spherical crystals are almost identical to those simulated for parallel-plate crystals whereas the shapes of the images for parallel-plate and spherical crystals completely differ. This reveals that the intensity distribution profiles in pinhole topographs depend on the size of the crystal but are almost uneffected by the shape of the crystal.

Al Haddad & Becker (1990) reported a detailed discussion about the primary extinction effect of X-rays in a spherical crystal in two-beam cases based on Kato's spherical-wave dynamical theory (Kato, 1961*a*,*b*). The spherical-wave dynamical theory gives the same wavefield as the result of the two-beam T–T equation solved under the boundary conditions of spherical-wave incidence. In Al Haddad & Becker (1990), it is found that complex considerations are needed when dealing with the behavior of X-rays in a spherical crystal, in which the diffraction geometries are categorized into three kinds of configuration. This complexity is due to the difficulty in considering the situation where the transmission (Laue) and reflection (Bragg) geometries coexist. This complexity can be avoided by the simple procedure described in §2 of a separate paper (Okitsu *et al.*, 2011). The important point of this procedure is to let all values of $\chi_{h_i-h_j}$ in equation (8) of Okitsu *et al.* (2006) be zero when the position is outside the crystal but inside the 'virtual Borrmann fan' in the two-beam case or 'virtual Borrmann pyramid' in the *n*-beam case ($n \in \{3, 4, 5, 6, 8, 12\}$) when integrating the Takagi–Taupin equation.

The integrated intensities of X-rays reflected from a spherical crystal satisfying an *n*-beam condition fully bathed in the incident X-rays can also be estimated using the same procedure as described by Al Haddad & Becker (1990). First, the intensity distribution profile of **h**- or **g**-reflected X-rays in a pinhole topograph as shown in Figs. 1(*c*) and 1(*d*) is to be integrated to obtain the 'total reflected intensities'. The 'total reflected intensities' are further integrated by scanning two-dimensionally the position of the incidence point r_e to obtain the integrated intensity. The position of r_e should be scanned over a plane whose distance from S_c is equal to the radius of the crystal in such a range that any portion of the crystal is inside the 'virtual Borrmann pyramid'.

The present work was performed at the High-Power X-ray Laboratory, Nano-Engineering Research Center, Institute of Engineering Innovation, Graduate School of Engineering, The University of Tokyo, Japan. The computer simulations were performed using the facilities of the Supercomputer Center, Institute for Solid State Physics, The University of Tokyo, Japan. The present work is one of the activities of the Active Nano-Characterization and Technology Project financially supported by the Special Coordination Fund of the Ministry of Education, Culture, Sports, Science and Technology of the Japan government.

References

Al Haddad, M. & Becker, P. (1990). *Acta Cryst.* A**46**, 112–123.
Chang, S.-L. (1998). *Acta Cryst.* A**54**, 886–894.
Chang, S.-L. (2004). *X-ray Multiple-Wave Diffraction, Theory and Application.* Berlin: Springer.
Colella, R. (1995*a*). *Comments Condens. Matter Phys.* **17**, 175–198.
Colella, R. (1995*b*). *Comments Condens. Matter Phys.* **17**, 199–215.
Ishiwata, G., Okitsu, K. & Ishiguro, M. (2010). *Acta Cryst.* A**66**, 484–488.
Kato, N. (1961*a*). *Acta Cryst.* **14**, 526–532.
Kato, N. (1961*b*). *Acta Cryst.* **14**, 627–636.
Okitsu, K. (2003). *Acta Cryst.* A**59**, 235–244.
Okitsu, K., Imai, Y., Ueji, Y. & Yoda, Y. (2003). *Acta Cryst.* A**59**, 311–316.
Okitsu, K., Yoda, Y., Imai, Y. & Ueji, Y. (2011). *Acta Cryst.* A**67**, 550–556.
Okitsu, K., Yoda, Y., Imai, Y., Ueji, Y., Urano, Y. & Zhang, X. (2006). *Acta Cryst.* A**62**, 237–247.
Shen, Q. (2005). *Adv. Imag. Elec. Phys.* **134**, 69–112.
Weckert, E. & Hümmer, K. (1997). *Acta Cryst.* A**53**, 108–143.
Weckert, E. & Hümmer, K. (1998). *Cryst. Res. Technol.* **33**, 653–678.